Corner Separation Zone Response to Plasma Actuation in the Hypersonic Boundary Layer over a Compression Ramp

Brock Hedlund, Alec Houpt, Stanislav Gordeyev, and Sergey Leonov
Institute for Flow Physics and Control, Department of Aerospace and Mechanical Engineering, University of Notre Dame, Notre Dame, IN, 46556

The characterization of the M=4.5 flow over a 2D model with a 30º compression ramp was performed at low enthalpy (T0=300K) and high enthalpy (T0=800-1250K) conditions for various Reynolds numbers. The impact of a pulse periodic plasma generated upstream of the ramp on the spectra of gas pressure/density oscillations was explored. Three measurement techniques were employed to characterize this oscillatory structure: a high frequency Shack-Hartmann wavefront sensor (aero-optical method), high frequency PCB pressure sensors, and a laser differential interferometer. Spectra of the flow oscillations measured by all three methods offer complementary results in characterizing dominant frequencies within the flow. Of these measurement methods, Shack-Hartmann is shown to be the most suitable tool for analysis of the flow spectra. Aero-optical measurements indicate flow structure modification due to variation of Re number and during plasma actuation. Under conditions of this test, further characterization by the Shack-Hartmann sensor at individual points in the flow has shown three modes of interaction depending on the Reynolds number: turbulent, transitional, and laminar, where the modes are mostly governed by freestream perturbations. The spectral measurements during plasma actuation indicate evidences of change in the dominant frequencies and amplitudes of perturbations from the natural state that occur over the separation region of the compression ramp.

I.   Introduction

Methods of supersonic and hypersonic boundary layer flow control by electrical discharges have previously been studied extensively [1, 2, 3, 4], showing a plausible controlling effect due to a non-uniform localized heating of the near surface gas layer. Specifically of interest to this study is the effect of a pulsed plasma actuator on the downstream flow oscillations in a hypersonic corner separation zone, where preliminary studies have performed a brief characterization of the oscillatory flow structure within the corner separation zone and leading up to it [4, 5, 6]. The boundary layer over compression ramp geometries is of interest to fluid dynamicists because of its role in scramjet inlets for effective flow conditioning prior to combustion. A number of publications have shown that the generation of a streamwise vorticity within the flow (tripping) leads to an accelerated transition of the boundary layer to turbulence [7, 8, 9], which is desirable for both reduction of the boundary layer separation and fueling mixing further downstream. It was also shown [5], that the shallow cavity discharge is a suitable method for generation of high frequency fluctuations in the flow, when operated at repetition frequencies greater than those of naturally occurring perturbations in the flow field.

The nature of the naturally occurring perturbations in the flow field over a compression ramp has been discussed in many studies [10, 11, 12, 13, 14]. This discussion revolves around the evolution of perturbations over a flat plate, which occurs in a different manner than subsonic and lower supersonic cases. In this case (adiabatic wall), second mode instabilities (of acoustic nature) are known to be dominant and grow in the hypersonic boundary layer leading up to the corner separation zone. Within the separation zone, dynamics of the instabilities are quite complex, but their growth is known to be neutral with only discrete acoustic modes becoming excited [11]. Upon reattachment, the flow exhibits the largest growths in instabilities (above the ramp surface). An important feature of the current work is that it examines the flow conditions with a relatively high level of initial perturbations in the core flow, which are typical for most wind tunnel tests and for a natural flow in a tail of a leading vehicle or a dust-seeded flow. Characterization of such flows is challenging, the numerical simulation is difficult, and the resulting flow structure is not obvious [15, 16].

Measurements of the flow structure, with primary interest on the oscillations occurring in the separation zone, are performed by three diagnostic tools in this study:

1. A Shack-Hartmann wavefront sensor is used to determine the dominating frequencies of flow oscillations in the flow field near a corner separation zone. This was experimentally proven in [17]. Wavefront sensing is demonstrated

to be a proper candidate for non-intrusive high frequency aero-optic measurements in hypersonic conditions due to the expectation of spanwise uniformity in flow and the sensor's sole sensitivity to gas density gradients. In addition, the wavefront sensor is capable of providing high spatial resolution and up to 1 MHz frequency response, limited only by the imaging camera's technical capability.

2. The measurement of high frequency pressure perturbations by means of surface mounted pressure sensors, which has been employed experimentally in Ref. [18, 19, 20], for example. Using 1 MHz response PCB sensors, pressure perturbations along the surface of a model in a hypersonic boundary layer can be detected and analyzed spectrally.

3. Laser differential interferometry (LDI) has been proven to be an effective tool in supersonic and hypersonic research [21, 22, 23]. LDI is used to measure the phase difference between two beams which are orthogonally polarized. Given that everything in the setup of the LDI remains constant except for the flow, fluctuations in the optical path difference can be directly related to fluctuations in flow density. The simplest of LDI systems can measure frequencies of flow perturbations up to 1 MHz and optical path differences on the order of 10 nm and below depending on the set up. This makes it a suitable tool for spectral analysis of low density, high-speed flows where the oscillation frequencies can extend into the hundreds of kHz.

II. Experimental Methods

2.1. Test Arrangement

Tests were conducted in the hypersonic wind tunnel ACT-1 at the University of Notre Dame[24]. Different nozzle arrangements allow for testing at Mach 4.5, 6, and 9. This test was focused on M=4.5 conditions. The ACT-1 facility utilizes a DC arc heater to generate high enthalpy flow, simulating conditions experienced in low density hypersonic flight. In this test series, stagnation temperatures was ranged from $T_0 = 800\text{-}1250\ K$ (high enthalpy) or $T_0 = 300\ K$ (low enthalpy). Other relevant test conditions include unit Reynolds Number $Re_L \approx 4 \cdot 10^6\text{-}3 \cdot 10^7\ m^{-1}$ (low enthalpy) or $Re_L \approx 4 \cdot 10^5\text{-}2.5 \cdot 10^6\ m^{-1}$ (high enthalpy), and stagnation pressure $5.5\ bar > P_0 > 0.8\ bar$. The composition of the gas mixture (typically nitrogen or artificial air) is controlled through variation of pressures and injection port arrangement. Other flow characteristics for varying total pressures are shown in Table 2.1, with flow velocities determined by direct measurements taken by a Shack-Hartmann wavefront sensor [6], Reynolds number is calculated based on the model length from a leading edge to the ramp.

Table 2.1: Flow characteristics for cold and heated flow in ACT-1

Cold			At Nozzle Exit					
P0 (bar)	Mass Flow (kg/s)	T0 (K)	T (K)	Velocity (m/s)	a (m/s)	P (Pa)	ρ (kg/m³)	Reynolds Number
0.9	0.028	293	58	699	155	311	0.018	3.4E+05
1.5	0.037	293	58	699	155	518	0.030	5.7E+05
1.9	0.048	293	58	699	155	656	0.038	7.2E+05
2.5	0.060	293	58	699	155	864	0.050	9.5E+05
3.2	0.078	293	58	699	155	1106	0.064	1.2E+06
4	0.096	293	58	699	155	1382	0.080	1.5E+06
5.5	0.134	293	58	699	155	1900	0.110	2.1E+06
Hot			At Nozzle Exit					
P0 (bar)	Mass Flow (kg/s)	T0 (K)	T (K)	Velocity (m/s)	a (m/s)	P (Pa)	ρ (kg/m³)	Reynolds Number
1.5	0.020	1238	245	1437	319	518	0.007	5.4E+04
2.25	0.032	906	179	1229	273	777	0.015	1.2E+05
3	0.043	880	174	1211	269	1037	0.020	1.7E+05
3.25	0.049	835	165	1180	262	1123	0.023	2.0E+05

Fig. 2.1 presents layout of the test setup. The experimental configuration for testing includes a compression ramp model mounted in the test section of ACT-1 (see Fig. 2.2). The experimental model consists of a flat plate with a sharp

leading edge and lower surface at a fixed angle $\alpha = 15\,°$. The second wedge is interchangeable and is mounted on top of the flat plate to form the compression ramp at angle $\beta = 30°$. In total, the model measures: length $L = 229\,mm$, width $W = 102\,mm$, and height $H = 19\,mm$. Shown in Figs. 2.1 and 2.2 is the arrangement of pressure sensors in the model. They are flush mounted at the locations labeled CH1, CH2, and CH3 in Fig. 2.1 to provide measurements on the flat plate surface both in the boundary layer and within the corner separation zone.
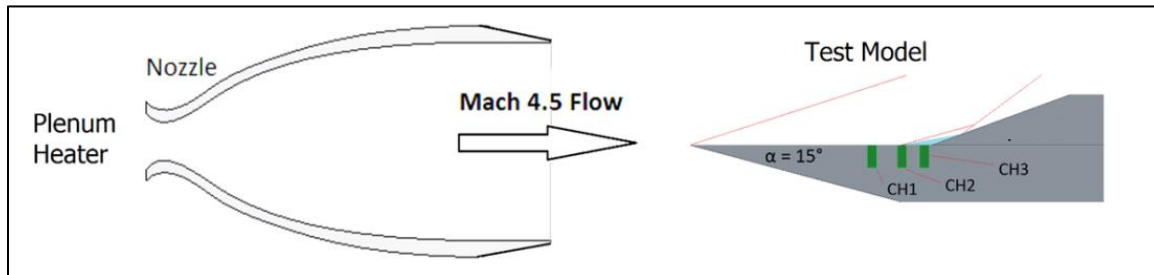
Figure 2.1.   Side view of experimental arrangement.
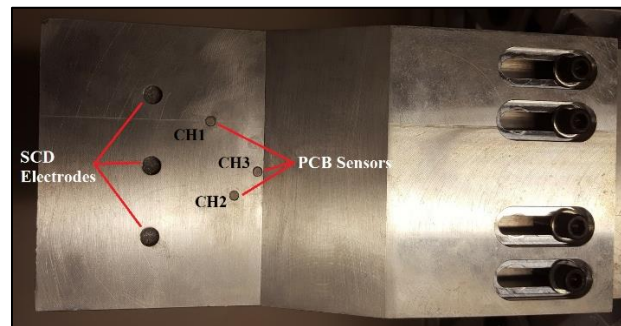
Figure 2.2.   Model in the test section of ACT-1 at the University of Notre Dame.

A high-resolution schlieren system was used to observe the basic flow structure, consisting of a pulsed NIR laser diode (Pulsed Laser Diode Module LS8-10-150-S10-00; 850 *nm*, 10 W peak power, 150 ns pulse duration) and a framing camera (Basler acA2040-180km-NIR, up to 187 frames per second at full 2k × 2k resolution). A typical frame has an exposure time of 24 *µs* with the laser pulse duration <1 *µs*, thus "freezing" the flow in time. Schlieren images indicate the presence of not only a separation zone in the corner, but also a region of large density gradients downstream, related to the compression shock wave. It is challenging to use schlieren visualization in such a low-density environment with a presence of a jet shear layer as was the case for this work. In order to increase the signal-to-noise ratio and improve the overall quality of the final image it was necessary to average tens or hundreds of images together. In Fig. 2.3 below, the average schlieren visualization clearly shows separation of the boundary layer and its associated shocks.
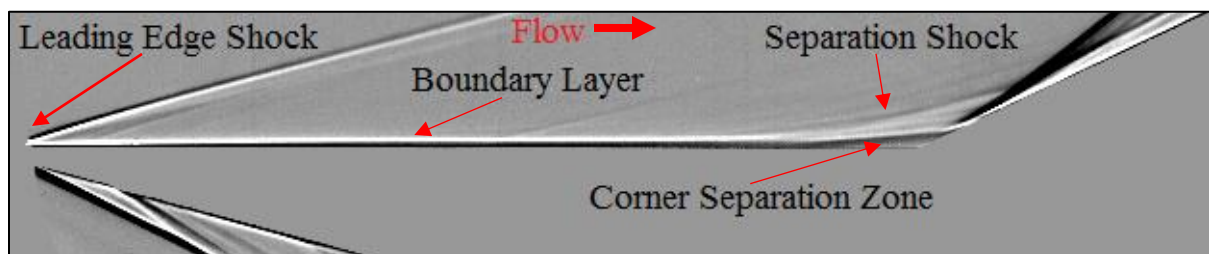

Figure 2.3.   Averaged schlieren image indicating important flow features.

2.2. Electrical Discharge

The Shallow Cavity Discharge actuator[25] was used to generate disturbances in the flow. The electrodes are arranged in small cavities, with no portion in the flow, existing a few millimeters in size, and are installed on the metallic surface of the model. It has the proper discharge geometry, reasonably low applied voltage, and a sufficient

level of the disturbances excited. Time resolved image of the SCD discharge in $M = 4.5$ flow taken by the Andor iStar ISSD camera is shown in Fig. 2.4 a. At $f = 50 - 100\ kHz$, the discharge works as a push-pull plasma mini-jet. A typical schlieren image, shown in Fig.2.4b, indicates that a heated in the plasma air is mostly flown over the corner separation zone. At lower frequencies of repetition the second operation mode was observed[25], currently considered as a cathode sheath pattern, where a rather thin layer of plasma covers most of the model surface. The cathode sheath is where a major part of the electric power is released[26] that is potentially beneficial for the BL control.
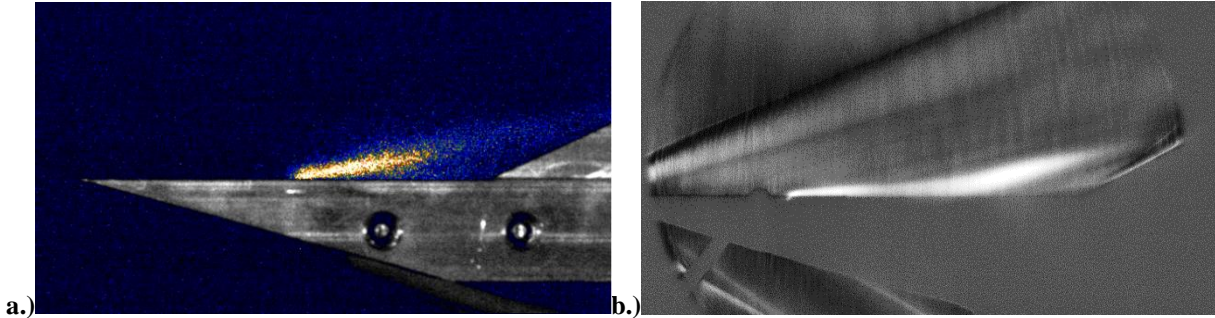

a.)   b.)

Figure 2.4.   SCD in $M = 4.5$, $Pst = 4\ mBar$ flow in plasma mini-jet operation mode; a.) camera image, exposure 1μs, delay time 3 μs (within the electric pulse); b.) time-averaged schlieren image.

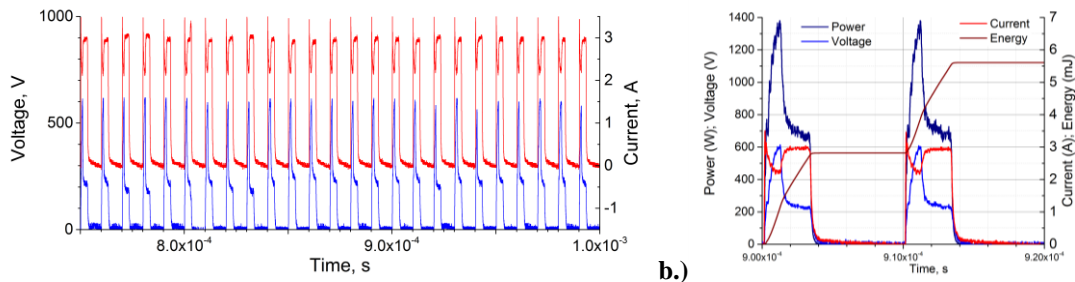a.)   b.)

Figure 2.5.   a.) Voltage –current time series of the SCD operation at $f = 100\ kHz$; b.) calculation of the discharge pulse power and energy for 3 SCDs.

Typical records of the electric parameters in M=4.5 flow are shown in Fig. 2.5a for a frequency of repetition $f = 100\ kHz$. The pulse energy and average power were calculated based on this data, as it is shown in Fig. 2.5b. The discharge parameters were as follows: frequency of repetition $f = 10 - 100\ kHz$; pulse duration $t < 4$ μs; voltage $U < 1\ kV$; pulse energy $E = 0.8 - 1.2\ mJ\ /unit$; average power $W_{av} < 400\ W$. Three units of SCD have been arranged in the model.

2.3. Flow Measurements

To characterize the perturbations in the flow field, a series of tests were carried out to collect the data by means three non-intrusive measuring systems. These include aero-optical measurements made by a Shack-Hartmann wavefront sensor, flush mounted surface pressure sensors, and LDI. Measurements of the flow dynamics are made in vicinity and within the separation zone to characterize high frequency responses and observe changes in the boundary layer separation within the ramp corner. Data collected within the separation zone was then compared with freestream measurements and baseline data to indicate differences in the spectra (see Figs. 2.7, 2.8, 2.10). In addition, the comparison between measurements made by surface mounted pressure sensors and a laser differential interferometer (LDI) will allow more comprehensive analysis of pressure and density dynamics within the flow than previously studied[5]. These measurement systems allow for flow observation without disruption of the highly sensitive flow structure.

1. Aero-optical measurements were performed using a high-speed Shack-Hartmann wavefront sensor[27, 28], the layout is shown in Fig. 2.6. The system consisted of a laser beam expanded to a 50-mm-diameter collimated beam and passed along the spanwise direction over the corner region of the model mounted in the test section. The spanwise beam propagation was chosen for two reasons. First, the flow is expected to be primarily spanwise-uniform. Second,

as the beam traverses the 4-inch-long region of the flow, aero-optical distortions become stronger thus improving the signal-to-noise ratio [28]. After exiting the test section, the beam is reflected off the return mirror, which sends the beam back along the same path. This so-called double-path setup further amplifies the aero-optical signal by a factor of two, as the beam traverses through the flow of interest twice, and also simplifies the optical setup. The returning beam is split off using a cube beam splitter, sent though a contracting telescope, which reduces the beam size to 12.5 mm in diameter, and recorded by a Phantom v1611 high-speed digital camera. The camera had a 38 mm focal length, 70×60 lenslet array with 0.3-mm-pitch, 100% fill ratio, attached to it. After passing through the lenslet array, the beam was split into sub-aperture beams and focused on the camera sensor, creating a series of dots. To achieve the high, 531 kHz, sampling rate, only a small portion of the image (128×64-pixel) was acquired for the full duration of the wind tunnel run. More details are considered in Refs.[29, 30].
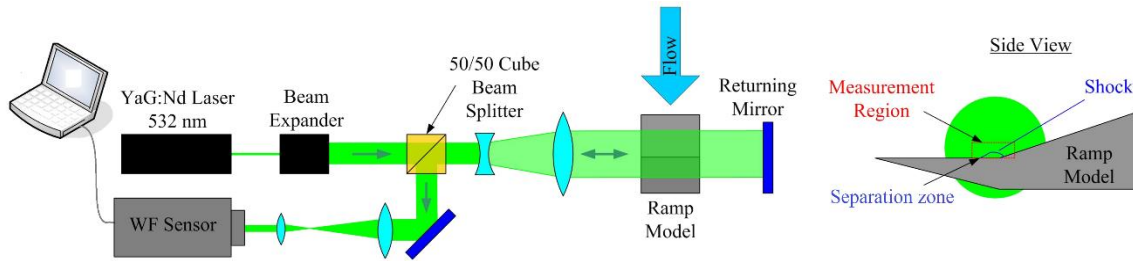

Figure 2.6.   Scheme of Shack-Hartmann wavefront sensor.

Spectra of flow perturbation acquired by the Shack-Hartmann sensor was analyzed at different points within the dot matrix (similar to shown in Fig. 3.1) to identify the spectra of flow perturbations and dominant frequencies of oscillations occurring in the flow (see Fig. 2.7). The non-dimensional frequency, defined by $f \cdot \delta / U_\infty$, allows for simple frequency analysis and comparison[31, 32]. Here, f is the perturbations frequency, δ is the boundary layer thickness, and U_∞ is the freestream velocity. The boundary layer thickness was chosen as a scaling factor to match expected length scales of dominating acoustic waves trapped inside the boundary layer. Values of dominant frequency within the separation zone for cold and hot flow range from $f \cdot \delta / U_\infty = 0.15$-$0.20$. This form functionally removes the shift of frequency that occurs between varying freestream unit Reynolds numbers seen previously[6]. The shift occurred as the result of differing boundary layer thicknesses at each Reynolds number and streamwise location. In Fig. 2.7, the freestream condition represents a point in the dot matrix measured in the core flow far from the surface of the model. The corner condition represents the point closest to the corner (<1 mm above the surface; <1 mm in front of the ramp tip). This point indicates a clear reduction in the amplitude of oscillations from the freestream condition at frequencies below 0.17. This appears as a "peak" in the data shown in Fig. 2.7. Both of these conditions are compared with the baseline signal as well. The narrow, high-amplitude peaks observed in the data are attributed to a digitizing noise and have to be neglected in the analysis. The signal-to-noise ratio is a quite high for the cold flow and has a reasonable magnitude in the low-density heated flow.
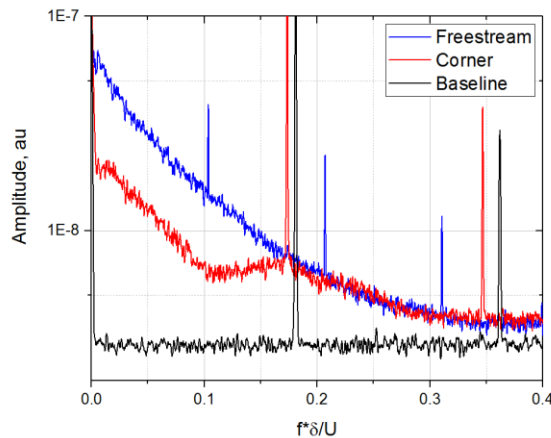

Figure 2.7.   Spectra of Shack-Hartmann data measured at the ramp corner and in the freestream, compared with the baseline with no flow ($Re \approx 3.4 \cdot 10^5$, $T_0 = 300$ K).

2. PCB™ (132 series) microsensors provided high frequency pressure measurements along the model surface in the corner separation zone and leading up to it. With a response frequency of up to 1 *MHz*, these piezo-electric transducers are capable of detecting weak shocks and high frequency perturbations impacting the sensor's diaphragm. Pressure spectra collected from the sensor provided reinforcing evidence to indicate the dominant natural frequencies present in both high and low enthalpy flows. Three sensors were located upstream of the ramp corner, with the sensing element mounted flush to the model's top surface. Along the flow axis, the sensors labeled CH1, CH2, and CH3 were mounted 20 mm, 10 mm, and 2.5 mm upstream of the ramp corner respectively, illustrated in Fig. 2.1. This spacing allowed for measurement of the flow pressure perturbations in the corner separation zone (CH3), near the flow separation point (CH2), and within the boundary layer upstream (CH1). Schlieren images verify the location of separation and existence of the separation zone within the corner. The sensors and their cables were carefully insulated to reduce vibrational noise from the model and electromagnetic noise from surrounding electronics. Fig. 2.8 below indicates a similar trend in the spectra compared to the Shack-Hartmann sensor results. With the exception of small spikes (due to EM noise, mainly in baseline condition), the primary feature in the pressure spectra is a peak existing at 0.17, measured at CH3. The signal-to-noise ratio has a reasonable magnitude in most cases without the plasma generation. The noise level appears to be extremely high at operation of high-voltage high-frequency power supply of the plasma generator.
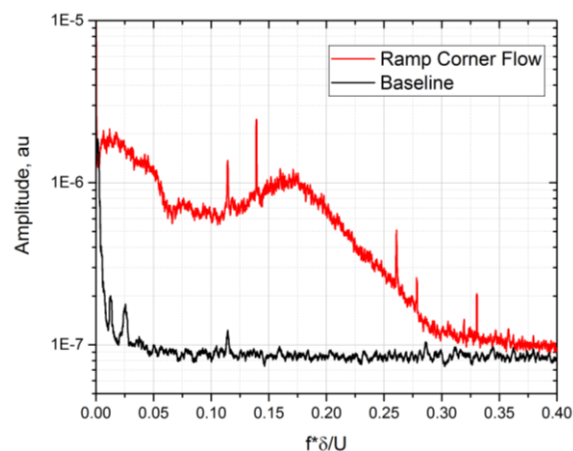

Figure 2.8.   **Spectra of pressure perturbations collected by PCB's, compared to baseline without flow**
($Re \approx 3.4 \cdot 10^5$, $T_0 = 300$ K).

3. Laser Differential Interferometry (LDI). A Melles-Griot linearly polarized He-Ne laser is used as the coherent light source. It passes through a quarter-wave plate with the ordinary and extraordinary axes aligned at 45° to the axis of polarization of the laser in order to produce circularly polarized light. The circularly polarized light passes through a Wollaston prism to produce two orthogonally polarized beams of equal intensity, with some constant phase shift, which are diverging from each other at 2°. The Wollaston prism is at the focal point of a 1 m focal length lens such that the orthogonally polarized beams are parallel to each other. The beams then pass through the test section with one beam isolated from the flow disturbances and the other passing through the boundary layer directly over the PCB inside the separation zone (CH3). The difference in density along the beam integrated path, where the beams passes through, introduces some new phase shift. An identical 1 m focal length lens focuses the beams back to a point on another Wollaston prism. This combines the beams into elliptically polarized light. The beams are interfered with a linear polarizer at 45° and the beam is imaged onto a photodiode. The intensity measured by the photodiode depends on the interference of the beams. The constructive/destructive interference is governed by the phase shift introduced by the density perturbations in the flow. The limits of the system are noise introduced (vibrational, ambient light, etc.), the response time of the photodiode, and the measurement circuit used.
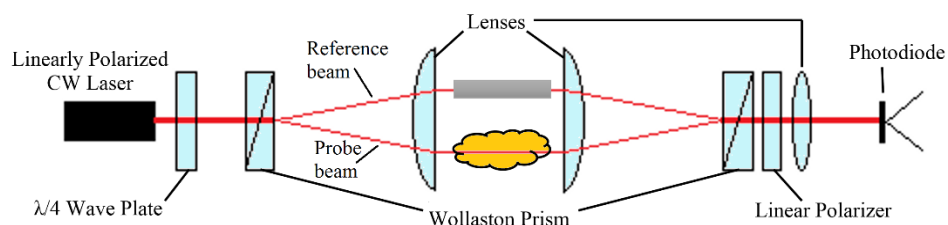
Figure 2.9.   Basic schematic of the laser differential interferometer.

Measurements taken by LDI further validate the Aero-optical and PCB data. For comparison, baseline and freestream tests are shown in Fig. 2.10 to compare with measurements taken in the corner separation zone. It is evident that the measurements taken in the corner separation zone indicate the same peak dominant frequency of 0.17 present in the Aero-optical and PCB data (*~60kHz* in frequency domain), perturbations existing both above and below this frequency are damped from the freestream case. Low-frequency peak in the LDI baseline spectra is caused by the facility mechanical vibrations.
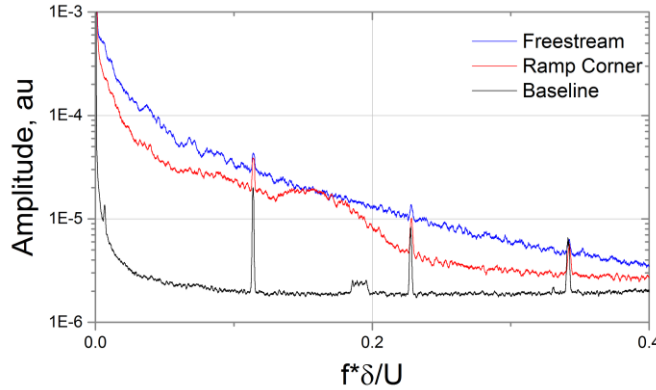

Figure 2.10.   Spectra of LDI data measured at the ramp corner and in the freestream, compared with the baseline with no flow.

Figure 2.11 presents the comparison of the spectra acquired by three measurement methods. These tests were carried out for the lowest Reynolds number case ($Re \approx 3.4 \cdot 10^5$) in $T_0 = 300\ K$ (low enthalpy) flow to ensure laminar flow over the model. Spectra presented in the plots in Figs. 2.7-2.11 display the amplitude of perturbations in arbitrary units, which allow for the normalization of the PCB and LDI data for comparison with the Shack-Hartmann data. Evidence of turbulence exists within LDI results at higher Re due to the similarity in form to the freestream case and lack of any distinguishable dominant frequency. It is believed that a turbulent shear layer exists at the edge of the flow, which effectively masks any dominant frequency detectable over the model by the LDI system. The flow configuration is a free jet for which a turbulent shear layer is expected to develop at high Re. The LDI is a path integrated system and measures differences in densities in the spanwise direction. Therefore the LDI is unable to distinguish between disturbances which are in the separation zone and those which would exist in a turbulent shear layer. The Shack-Hartmann system does not run into this same issue, as it measures disturbances occurring in the streamwise and wall normal directions. The PCB pressure sensors are a pointwise measurement and are unaffected by this consideration. A focused LDI system may be able to resolve this issue, but the 2-D planar geometry of the compression ramp makes it difficult to implement. In Fig. 2.11, the frequency content of the LDI data below and above the dominant frequency differs from that obtained with the Shack-Hartmann wavefront sensor. The LDI system is more susceptible to low frequency external effects, such as optical table vibrations, than the Shack-Hartmann system. These external effects along with higher sensitivity to disturbances in the shear layer contribute to the elevated amplitudes of the oscillations at frequencies below the dominant frequency as compared to the aero-optical data. The amplitude of the LDI frequency spectrum is slightly lower than that of the Shack-Hartmann at frequencies higher than the dominant frequency, and the PCB data has an amplitude much lower than both. The PCB has a lower effective level of the noise threshold and is collecting data at a single point while the two optical methods are path-integrated. Once plasma actuators are implemented, the use of pressure sensors becomes problematic due to the high level of electromagnetic noise generated by the discharge. Thus, in the case of characterizing the fluctuations for the planar hypersonic compression ramp, the Shack-Hartmann wavefront sensor has shown to be the most effective tool for data collection due to its high temporal resolution, ability to collect spatially resolved data over a region, and its relative insensitivity to perturbations present in the freestream outside of the region of interest.
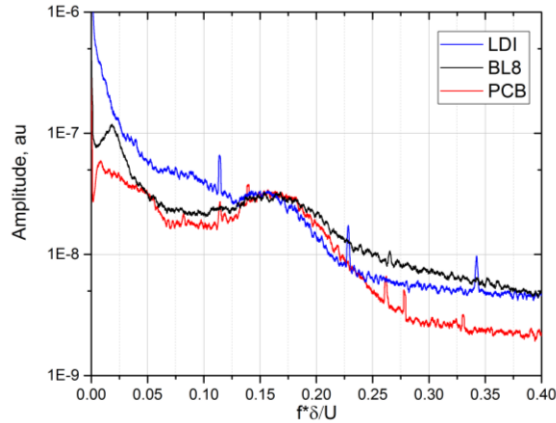
Figure 2.11.   **Spectral data comparison: Shack-Hartmann wavefront sensor (BL8, see Fig. 3.5 for location), pressure sensors (PCB), and LDI.**

III.   Experimental Results

Initial characterization of the flow by three methods in this study has shown the Shack-Hartmann wavefront sensor to be the most suitable tool to analyze the state of the BL, including dominant frequencies within the flow spectra, in the case of electromagnetic noise. The flow structure can be further analyzed by individual regions within the flow. Figure 3.1 shows the field of measurements performed by the Shark-Hartman sensor. There are four lines with ten points in each. A few corner points are masked by the model ramp. The X and Y distance between the points is 1.2 mm.
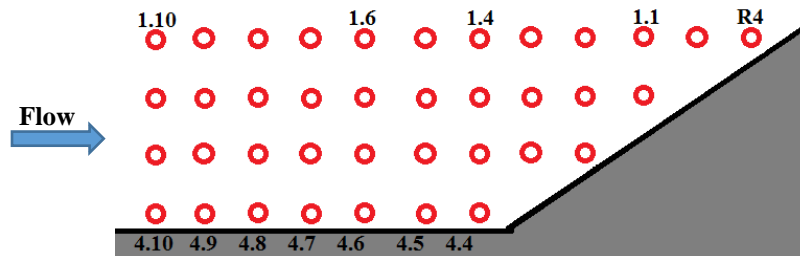

Figure 3.1.   Dot matrix of Shack-Hartmann measurement locations; 1.2 mm between points.

Figure 3.2 shows spectra of the flow along two line profiles at high and low Re in low enthalpy ($T_0 = 300\ K$) flow. The line profile closest to the wall (4.4 – 4.10) indicates a decrease in the amplitude of fluctuations as flow approaches the corner of the ramp (Fig. 3.2a). There is no noticeable effect far from the wall in Fig. 3.2b. It is important to note that point 1.1 locates downstream of the compression shock, which accounts for the increase in amplitude from 1.10 and 1.6. At high Re, the amplitude of disturbances increases as the flow travels downstream and is coupled with a lack of distinguishable flow features in the frequency domain. The steady decay in fluctuations at all points shown in Figs. 3.2c,d may indicate the presence of turbulent flow throughout the flow at this high of Re.
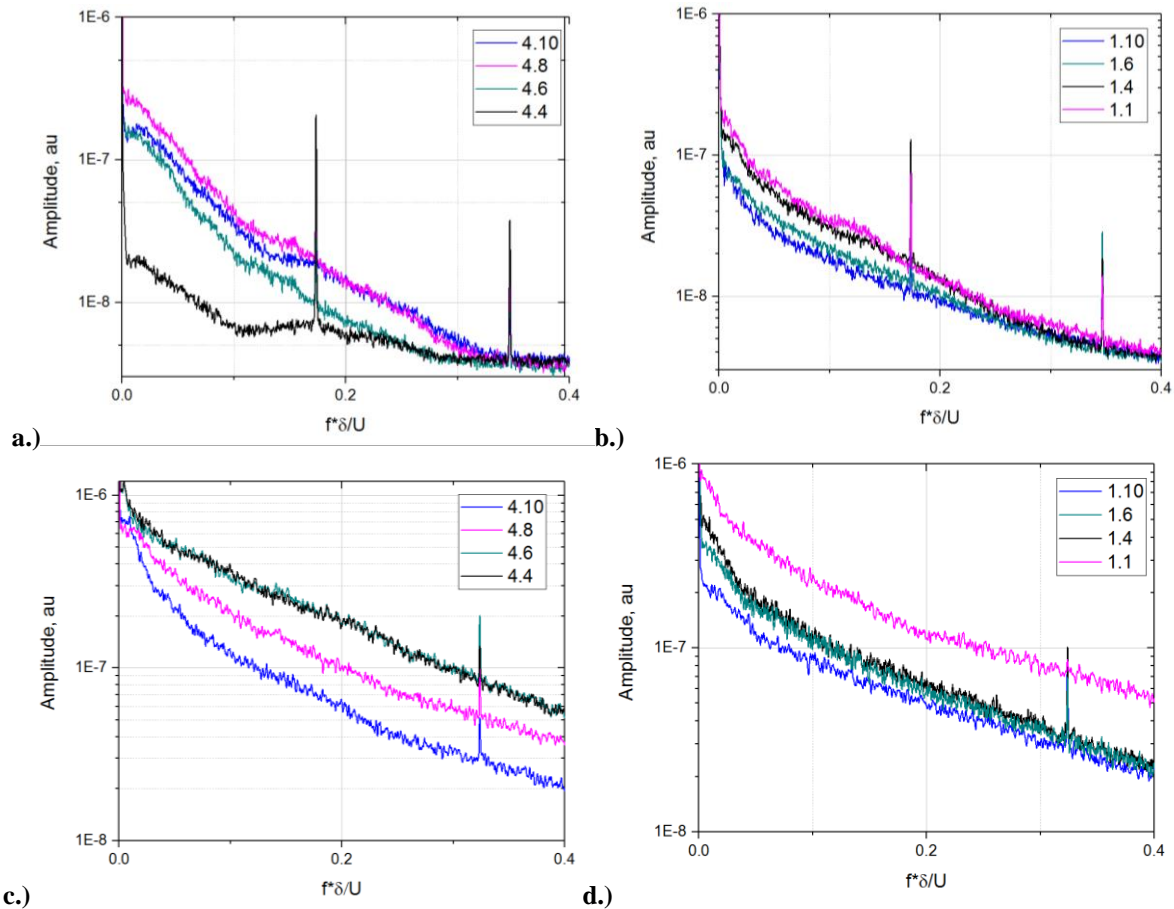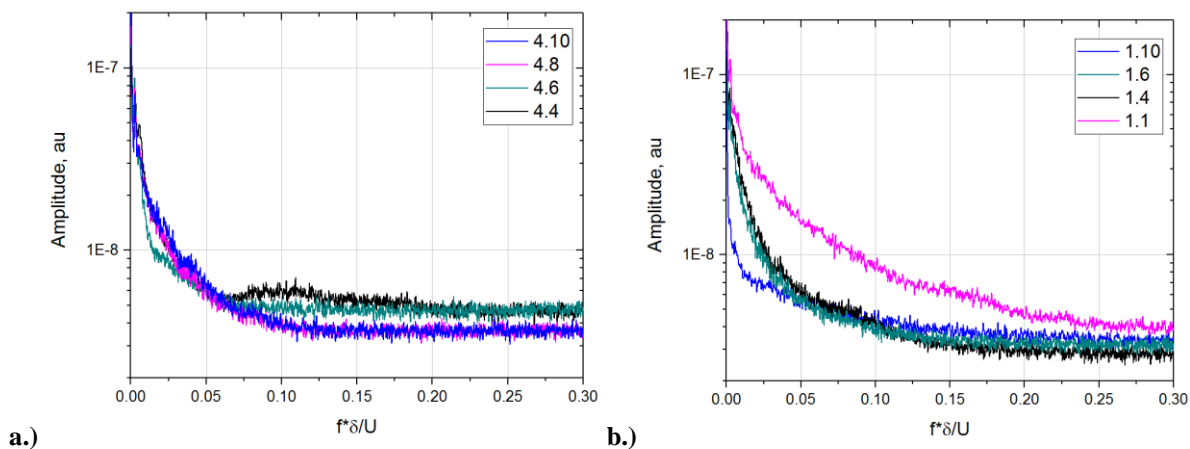
Figure 3.2. Spectra of Shack-Hartmann data for low enthalpy flow ($T_0 = 300\ K$); a. b.) $Re \approx 5.7 \cdot 10^5$; c. d.) $Re \approx 2.1 \cdot 10^6$.

The same measurements were collected for high enthalpy flows ($T_0 = 1238\ K, 835\ K$), for relatively low and high Re cases. In this situation, the line profile along the wall (Figs. 3.3a,c) indicates the presence of a raised peak in the spectra occurring downstream (in the ramp corner). Figure 3.3c indicates a damping of fluctuations in the ramp corner at frequencies below 0.14 and amplification of higher frequencies. Far from the wall, downstream locations exhibit the largest fluctuations with few distinguishable features in the spectra, similar to the low enthalpy flow cases.
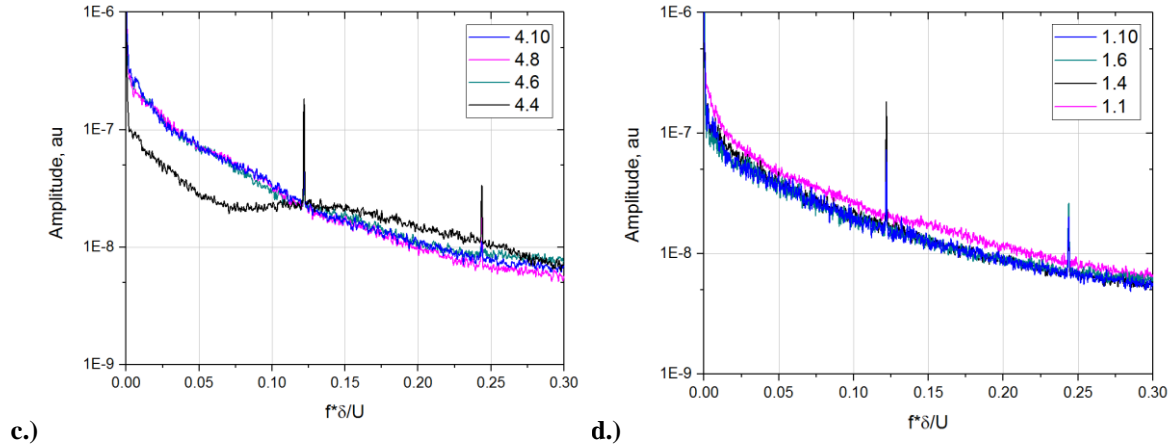
Figure 3.3. Spectra of Shack-Hartmann data for high enthalpy flow; a. b.) $Re \approx 5.4 \cdot 10^4$ ($T_0 = 1238\ K$); c. d.) $Re \approx 2.0 \cdot 10^5$ ($T_0 = 835\ K$).

The boundary layer conditions were characterized based on features of flow perturbation spectra. Figure 3.4 presents the data in terms of the Power Spectral Density (PSD), which was defined as $PSD = \check{\rho}^2 \cdot f, [Hz^{-1}]$, where $\check{\rho}$ is a component of the optical density perturbation measured by the Shack-Hartmann sensor in relative units, f is the frequency of perturbations. However, this approach is not strong enough to compare the data from the Shack-Hartmann sensor to the pressure sensors data [17, 33]. The data are shown for three cases: (a) P0=5.5 Bar, $Re \approx 2.1 \cdot 10^6$; (b) P0=1.5 Bar, $Re \approx 5.7 \cdot 10^5$; and (c) P0=1.5 Bar, $Re \approx 5.4 \cdot 10^4$ (high enthalpy). In all these cases the graphs are shown for free stream point 1.10 (see Fig.3.1); close to the ramp point 1.1; in the boundary layer 4.9 which is far upstream from separation zone; and in the separation zone point 4.4. Note, the increasing of the baseline with frequency indicates that the system is close to the sensitivity limit.
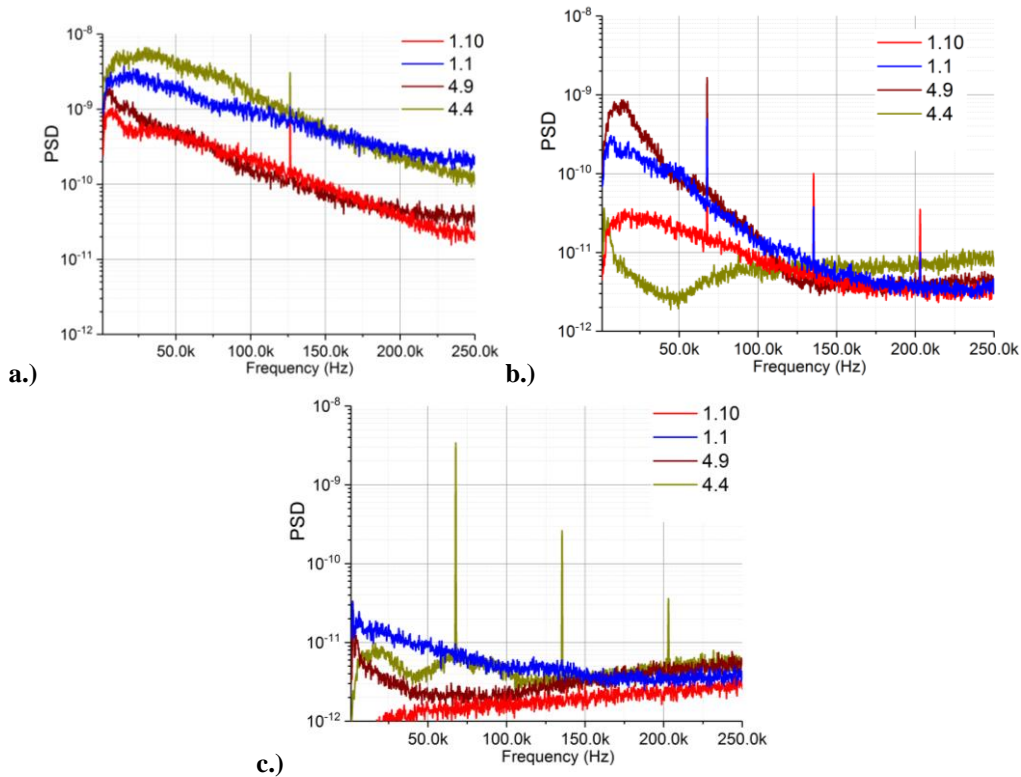

Figure 3.4. Power Spectral Density of flow perturbations for a.) P0=5.5 Bar, $Re \approx 2.1 \cdot 10^6$; b.) P0=1.5 Bar, $Re \approx 5.7 \cdot 10^5$; and c.) P0=1.5 Bar, $Re \approx 5.4 \cdot 10^4$.

In case (a) the level of flow perturbations is high compared to other cases. The PSD could be attributed to turbulent flow in the freestream (point 1.10) and in the BL (point 4.9). The intensity increases even more near the ramp due to effect of the separation-related shock. Amplitude of perturbations in the separation zone is high with dominance at relatively low frequencies f<100kHz. In case (b) the freestream spectra looks similar to case (a) except for the amplitude, which is approximately ρ^2 times lower. Contrary to case (a), the intensity of perturbations rises in the boundary layer but is significantly damped in the separation zone. At the lowest Re in case (c), the freestream perturbations were lower than the detection threshold, demonstrating significant rise on the ramp and in the separation zone. Based on the spectra at location 4.9, the boundary layer is laminar. The spectra at location 4.4 indicates a presence of dominant frequencies with increased magnitude, which could be attributed to development of the acoustic instabilities. Based on the criteria described in Ref [12, 13]

$$\varepsilon_M - \frac{\beta Re_L^{1/4}}{(M_\infty^2 - 1)^{1/4}} \tag{1}$$

is equal to $\xi \approx 3$ and this mode should experience "separation with distorted friction". Apparently, the increase of the Reynolds number in the current configuration and a significant level of initial disturbances in the flow do not cause a secondary separation but leads to the turbulent transition.

Shack-Hartmann data was also collected for low and high enthalpy tests at the lowest Re conditions possible for the facility in order to maintain laminar flow to study then how plasma actuation may be applied. These consisted of $Re \approx 3.4 \cdot 10^5$ (low enthalpy flow); and $Re \approx 5.4 \cdot 10^4$ (high enthalpy flow). These results reinforce previous characterization of the perturbations present in the hypersonic boundary layer[5]. The analysis provided shows that the same dominant natural frequency is detected as it is presented in Fig. 3.5. The location of points BL1 – BL9 in Fig. 3.5b,c correspond to locations in the flow field where Shack Hartmann measurements were taken. These can be referenced to Fig. 3.5a, illustrating the points of measurement in relation to the compression surface, being similar to the line 4 in Fig.3.1. The physical dominant frequency appears to be significantly higher for high enthalpy tests. This can be explained by two effects. The more dominant effect is due to decrease in Reynolds Number during the high enthalpy tests. The second is due to the adiabatic effect of the wall and corresponding reduction of boundary layer thickness. Since arc heating during high enthalpy tests greatly increases the flow temperature in relation to the wall, there exists a mode of heat transfer between the flow and wall. In the low enthalpy tests, the wall is approximately adiabatic, whereas the high enthalpy tests do not exhibit an adiabatic behavior with the wall due to the short run time. Therefore, the higher enthalpy tests produce a relatively thinner boundary layer capable of experiencing higher disturbance frequencies. This pathway however, is difficult to detect due to complexity of changes in the velocity, density, and pressure. The dimensional dominant frequency in the low enthalpy flow corresponds to *55 kHz* and in the high enthalpy flow, it is *110 kHz*, approximately. It is notable that, in terms of dimensionless frequency, the value for the acoustical trapped wave is almost the same for low and high enthalpy cases. From the Fig.3.5, the points measured closer to the corner position indicate higher frequency amplitudes up to some distance (BL6) and then it is damped similar to one shown in Fig.3.4.
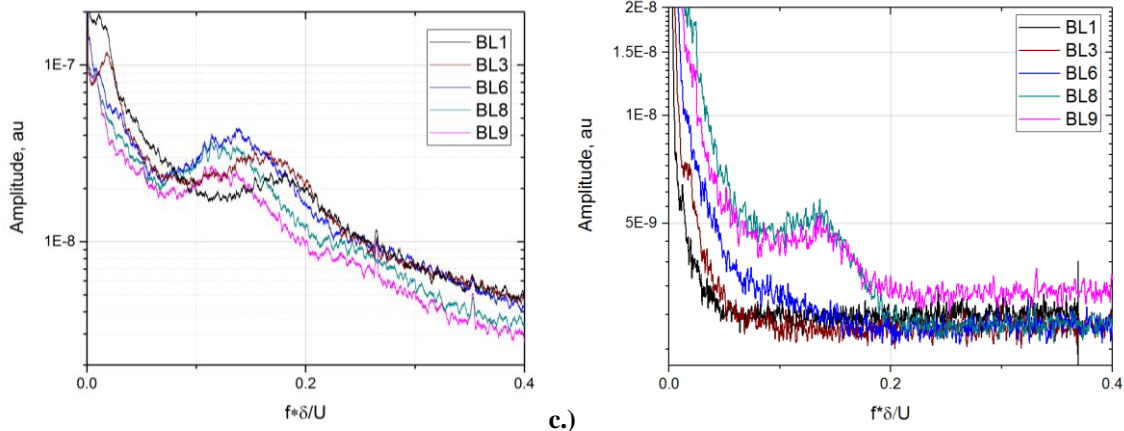

a.)

b.)   **c.)**
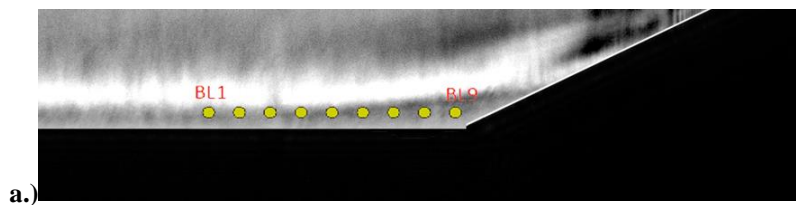
Figure 3.5.   a.) Measurement locations, 1.2 mm between points; Spectral data collected by Shack-Hartmann wavefront sensor from b.) low enthalpy test (T= 300 K, $Re \approx 2.0 \cdot 10^5$); and c.) high enthalpy test (T= 1238 K, $Re \approx 5.4 \cdot 10^4$).

The effect of pulsed plasma actuation at a dimensionless frequency of 0.256 (100kHz repetition rate) on the dominant frequencies in the spectra is shown in Fig. 3.6. Points of interest include 4.7 and 4.4 along the model wall leading up to the corner, where a small plasma effect appears to exist. Higher amplitude fluctuations during plasma actuation at location 2.4 may indicate a shift of the separated boundary layer due to expansion and contraction of the separation zone. Point R4, located near the root part of the shock generated by the ramp shows a significant response to the plasma actuation. This effect, shown in Fig. 3.6d exists as an amplification of flow disturbances for all observed frequencies. Point R4 is approximately where the boundary layer reattaches to the ramp and this location is often the location of transition from a laminar to turbulent boundary layer[11]. At the same time, the effect is negligibly small in the BL and in the separation area.
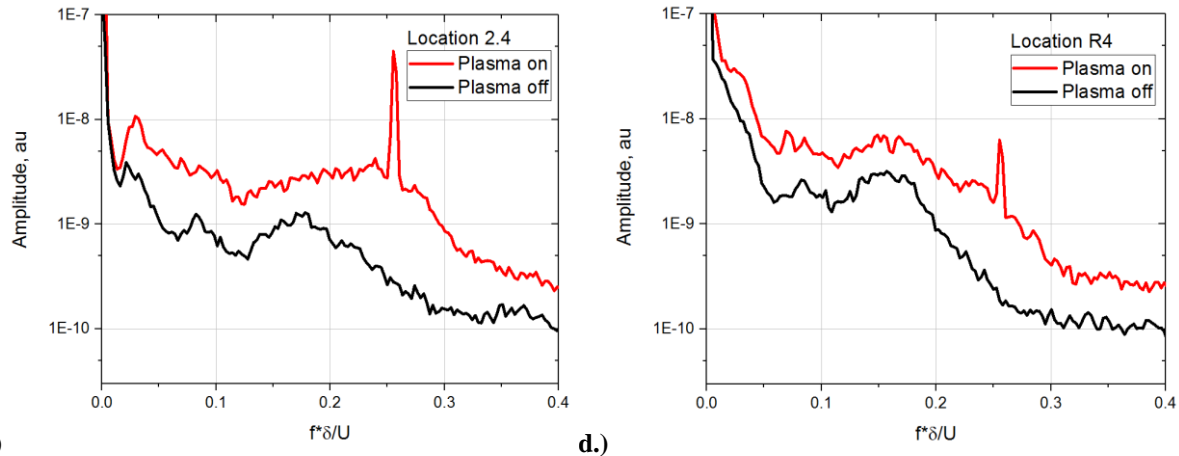

a.)   **b.)**

c.) **d.)**
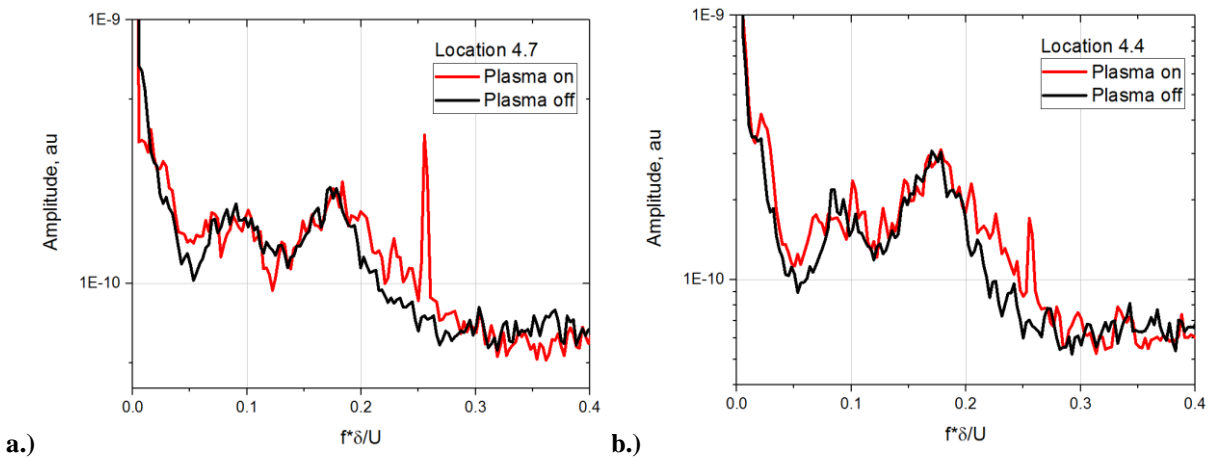
Figure 3.6. **Spectra of flow disturbances. Y-component of the deflection-angle spectra, plasma excitation $f = 100\ kHz$; a.) location 4.7; b.) location 4.4; c.) location 2.4; d.) location R4.**

IV. Summary

Measurements of the disturbances present in a hypersonic boundary layer and in a corner separation zone via the aforementioned methods provide a better understanding of the airflow pressure and density dynamics occurring within the geometry of a planar hypersonic compression ramp. Optical methods are especially useful in this environment as they are nonintrusive ones of obtaining spatially and temporally resolved data. Of the methods employed, Shack-Hartmann wavefront sensing proved to be the best for the study of this flow due to its ability to collect temporally resolved streamwise and wall normal data at many points in the flow field. It is also relatively insensitive to vibrations and electromagnetic noise and quick to employ compared to other optical diagnostics. Schlieren imaging provides a visualization of the flow structure and can be used to study behavior of boundary layers and shock waves. Laser Differential Interferometry provides high frequency measurements similar to Shack-Hartmann, but measures phase differences in the spanwise direction and is not ideal for flows with shear layers outside of the region of interest. While spectral data from these optical methods are the result of measurements in the density gradient within the flow, pressure perturbations at the surface can also be measured by surface mounted sensors. Each of these methods detected the same dominant frequency present in the boundary layer/separation zone and therefore reinforce the results obtained via each method. Further characterization by Shack-Hartmann indicates the transition to turbulence occurs at higher Re in the freestream, and in some cases, in the BL. In laminar flow, the presence of acoustic instabilities is shown in the separation zone, which may experience damping in some cases. It was shown that plasma actuation has a significant effect at multiple points in the flow field and proves to be a robust technique for promoting laminar-to-turbulent transition of the boundary layer near flow reattachment in the ramp configuration. Future work will focus on studying what flow conditions are most receptive to plasma actuation and what geometries/actuator locations can be most effective in introducing and promoting flow instabilities.

Acknowledgments

References

[1]   J. Kriegseis, B. Simon, S. Grundmann, "Towards In-Flight Applications? A Review on Dielectric Barrier Discharge-Based Boundary-Layer Control," Applied Mechanics Reviews, Vol. 68, 020802-1, 2016.

[2]   S. Im, H. Do, M. A. Cappelli, "The Manipulation of an unstarting supersonic flow by plasma actuator," Journal of Applied Physics D: Applied Physics, 45, 485202, 2012.

[3]   J. Shin, "A study of direct-current surface discharge plasma for a mach 3 supersonic flow control," Ph. D. Dissertation, Department of Aerospace Engineering and Engineering Mechanics, University of Texas at Austin, Austin, TX, 2007.

4   K. Lin, H. Yan, "Numerical simulation of supersonic shear layer with plasma actuator," Procedia Engineering, Vol. 126, pp 44-48, 2015.

5   A. Houpt, B. Hedlund, S. Gordeyev, T. Juliano, S. Leonov, "Transient Plasma Impact on Spectra of Flow Disturbances in a Corner Separation Zone at Mach 4.5," AIAA Paper 2016-3807; AIAA Aviation 2016.

6   B. Hedlund, A. Houpt, S. Gordeyev, S. Leonov, "Measurement of Plasma Induced Flow Perturbations Affecting a Mach 4.5 Corner Separation Zone", AIAA Paper 2017-0154.

7   S. A. Berry, R. J. Nowak and T. J. Horvath, "Boundary Layer Control for Hypersonic Airbreathing Vehicles," in 34th AIAA Fluid Dynamics Conference, AIAA Paper 2004-2246, Portland, Oregon, 28 June-1 July, 2004.

8   S. Schneider, "Effects of Roughness on Hypersonic Boundary-Layer Transition," Journal of Spacecraft and Rockets, vol. 45, no. 2, pp. 193-209, 2008.

9   E. Reshotko and A. Tumin, "Role of Transient Growth in Roughness-Induced Transition," AIAA Journal, vol. 42, no. 4, pp. 766-770, April 2004.

10   I. Egorov, A. Fedorov, A. Novikov, V. Soudakov, "Direct numerical simulation of supersonic boundary-layer stabilization by porous coatings," in 45th AIAA Aerospace Sciences Meeting, AIAA Paper 2007-948, Reno, Nevada, 8-11 January, 2007.

11   I. Egorov, A. Novikov, A. Fedorov, "Numerical Modeling of the Disturbances of the Separated Flow in a Rounded Compression Corner," Fluid Dynamics, Vol. 41, No. 4, pp. 521-530, 2006.

12   V. Neiland, L. Sokolov, V. Shvedchenko, "Temperature Factor Effect on the Structure of the Separated Flow within a Supersonic Gas Stream", Fluid Dynamics, Vol. 43, No. 5, pp. 706-717, 2008.

13   G. Korolev, J. Gajjar, A. Ruban, "Once again on the supersonic flow separation near a corner", Journal of Fluid Mechanics, Vol. 463, pp. 173-199, 2002.

14   P. Balakumar, H. Zhao, H. Atkins, "Stability of Hypersonic Boundary Layers over a Compression Corner", Journal of Fluid Mechanics, Vol. 463, pp. 173-199, 2002.

15   X. Zhong, X. Wang, "Direct numerical simulation on the receptivity, instability and transition of hypersonic boundary layers," Annual Review of Fluid Mechanics, Vol. 44, pp. 527–561, 2012.

16   F. Qin, W. Xuesong, "Response and receptivity of the hypersonic boundary layer past a wedge to free-stream acoustic, vortical and entropy disturbances," J. Fluid Mech., Vol. 797, pp. 874–915, 2016.

17   J. Sontag and S. Gordeyev, "Non-intrusive Velocity and Density Measurements in Subsonic Turbulent Boundary Layer," AIAA Paper 2015-3247 in 46th AIAA Plasmadynamics and Lasers Conference, Dallas, Texas, 2015.

18   K. R. Raman, "Surface Pressure Fluctuations in Hypersonic Turbulent Boundary Layers," NASA CR-2386, February 1974.

19   M. Estorf, et al., "Surface-Pressure Measurements of Second-Mode Instability in Quiet Hypersonic Flow," AIAA Paper 2008-1153, 2008.

20   K. Casper, S. Beresh, J Henfling, and S Schneider, "Hypersonic Wind-Tunnel Measurements of Boundary-Layer Transition on a Slender Cone", AIAA Journal, Vol. 54, No. 4, April 2016.

21   G. Smeets, A. George and A. Translated by: Goetz, "Laser-Differential Interferometer Applications in Gas Dynamics," 1996.

22   T. Salyer, S. Collicott and S. Schneider, "Feedback Stabilized Laser Differential Interferometry for Supersonic Blunt Body Receptivity Experiments," in *38th Aerospace Sciences Meeting and Exhibit*, Reno, NV, 2000.

23   N. Parziale, J. Shepherd and H. Hornung, "Differential Interferometric Measurement of Instability in a Hypervelocity Boundary Layer," *AIAA Journal,* vol. 51, no. 3, pp. 750-745, 2013.

24   D. Baccarella, Q. Liu, A. Passaro, T. Lee, H. Do, "Development and testing of the ACT-1 experimental facility for hypersonic combustion research," Measurement Science and Technology, Vol. 27, (2016), 045902.

25   S. Leonov, A. Houpt and F. Falempin, "Control of Hypersonic BL Transition by Electrical Discharge (feasibility study)," AIAA Paper 2015-3602 in *20th AIAA International Space Planes and Hypersonic Systems and Technologies Conference*, Glasgow, Scotland, 2015.

26   Y. P. Raizer, Gas Discharge Physics, Berlin: Springer, 1991.

27   R. K. Tyson, Principles of Adaptive Optics, New York: Academic., 1997.

[28] J. Sontag and S. Gordeyev, "Non-intrusive Velocity and Density Measurements in Subsonic Turbulent Boundary Layer," in 46th AIAA Plasmadynamics and Lasers Conference, Dallas, Texas, 2015.

[29] A. Houpt, S. Leonov, S. Gordeyev and T. Juliano, "Optical Measurement of Transient Plasma Impact on Corner Separation in M=4.5 Airflow," Paper AIAA-2016-2160.

[30] J. Sontag and S. Gordeyev, "Non-intrusive Velocity and Density Measurements in Subsonic Turbulent Boundary Layer," AIAA Paper 2015-3247 in 46th AIAA Plasmadynamics and Lasers Conference, Dallas, Texas, 2015.

[31] V. Narayanaswamy, L. Raja, N. Clemens, "Control of unsteadiness of a shock wave/turbulent boundary layer interaction by using a pulsed-plasma-jet actuator," Physics of Fluids, 24, 07610 (2012).

[32] J. C. Gonsalez and D. S. Dolling, "Correlation of interaction sweepback effects on the dynamics of shock-induced turbulent separation," AIAA Paper 93-0776, 1993.

[33] J. Sontag and S. Gordeyev, "Studies of Density Fields in Non-Adiabatic Boundary Layers Using Wavefront Sensors," to be presented at AIAA conference, 5-9 June, Denver, CO, 2017.